ChemPubSoc Europe

DOI: 10.1002/batt.201900095

BATTERIES & SUPERCAPS Communications

Simultaneously Boosting the Ionic Conductivity and Mechanical Strength of Polymer Gel Electrolyte Membranes by Confining Ionic Liquids into Hollow Silica Nanocavities

Bishnu P. Thapaliya,[a, b] Chi-Linh Do-Thanh,[a] Charl J. Jafta,[b] Runming Tao,[a] Hailong Lyu,[a, b] Albina Y. Borisevich,[c] Shi-ze Yang,[d] Xiao-Guang Sun,*[b] and Sheng Dai*[a, b]

A central problem of solid polymer electrolytes is their inability to achieve robust mechanical strength with fast ionic conductivities required for commercialization of lithium metal batteries (LMBs). At present, state-of-the-art offers superiority of one at the expense of the other. Here, this dilemma has been solved by fabricating mechanically robust solid composite polymer electrolytes (SCPEs) with superior ionic conductivity (0.5 mS cm^{-1} at 20 °C) by confining ionic liquids (ILs) in the hollow scaffold offered by hollow silica (HS) nanospheres with unique architecture. Mechanical robustness was verified by the performance of a Li||Li symmetric cell cycling for extended hours without short-circuiting. In addition, SCPEs with HS have higher thermal and electrochemical stabilities than those without HS, due to strong interaction and coordination of HS nanoparticles with polymer and ionic liquids. Electrode compatibility and flexibility of the membrane could advance the LMBs technology.

The replacement of graphite by Li metal boosts the energy density of the current lithium-ion batteries (LIBs) because of high theoretical capacity (~3860 mAh g^{-1} or 2061 mAh cm^{-3}) and the lowest electrochemical potential (−3.04 V) of Li-metal.[1] However, challenges of the lithium anode such as Li dendritic growth, dead lithium, and rapid capacity degradation have hampered its commercialization.[1b,e] Different approaches such as using liquid electrolytes with additives,[2] morphological modification of anodes,[1b,2d, 3] and volume minimization[1b,4] have been explored, but could not completely solve the lithium dendrite problem as well as the accompanying safety concerns.

[a] B. P. Thapaliya, C.-L. Do-Thanh, R. Tao, H. Lyu, Prof. Dr. S. Dai
Department of Chemistry, Joint Institute for Advanced Materials,
University of Tennessee, Knoxville, TN 37996, USA
E-mail: dais@ornl.gov
[b] B. P. Thapaliya, C. J. Jafta, H. Lyu, Dr. X.-G. Sun, Prof. Dr. S. Dai
Chemical Science Division,
Oak Ridge National Laboratory,
Oak Ridge, TN 37831, USA
E-mail: sunx@ornl.gov
[c] A. Y. Borisevich
Center for Nanophase Materials Sciences,
Oak Ridge National Laboratory,
Oak Ridge, TN 37831, USA
[d] S.-z. Yang
Center for Functional Nanomaterials,
Brookhaven National Laboratory,
Upton, New York, 11973

Supporting information for this article is available on the WWW under https://doi.org/10.1002/batt.201900095

Solid-state electrolytes (ceramics and polymers) are the potential successors of the flammable liquid electrolytes as they offer better safety and device fabrication.[1b,f,3a,4–5] Inorganic ceramic electrolytes usually have high ionic conductivity with high elastic modulus to prevent Li dendrite growth, but they have low adhesion to electrodes, resulting in significant interfacial impedance.[1b,6] As a comparison, SPEs have low ionic conductivity and low elastic modulus not enough to prevent Li dendrite growth, but they are more flexible and have excellent adhesive properties along with better thermal, mechanical, and electrochemical stability. Therefore, they have received worldwide attention in generating high-performance LIBs and LMBs.[1b,7] So far, SPEs have not been applied in commercial batteries due to their low room temperature ionic conductivities.[8] To increase the ionic conductivity and suppress the crystallization of SPEs, approaches such as plasticizing, crosslinking, and synthesizing block copolymers have been explored.[9] However, none of them can simultaneously achieve high ionic conductivity and mechanically robust membranes.

It has been demonstrated that dispersing inorganic filler particles into the polymer matrix can enhance not only its mechanical strength but also its ionic conductivity because of a large interfacial surface area and amorphization of the polymer matrix.[10] Usually, two types of inorganic filler particles – inert fillers without lithium-ion conduction such as Al_2O_3, TiO_2, SiO_2 and active fillers with lithium-ion conduction such as Li_3N, lithium lanthanum zirconate (LLZO), lithium lanthanum titanate (LLTO), lithium lanthanum zirconium thallium oxide (LLZTO) etc. – can be used to fabricate solid composite polymer electrolytes (SCPEs).[8b,11] To further enhance the ionic conductivities of SCPEs, organic solvents have been used as plasticizers to form polymer gel electrolytes, which compromise their safety. As an alternative to organic solvents, ILs have been extensively investigated for application in LIBs due to their negligible vapor pressure, high ionic conductivity, electrochemical stability, and non-flammability.[12] Different strategies have been used to stabilize the lithium metal anode such as confinement of ILs into a biomimetic ant-nest silica architecture,[13] or mixing ILs with a different polymer or metal-organic-framework (MOF).[12f,14] However, the endless efforts to achieve mechanically robust membranes with high ionic conductivity are not paying off.

Our idea is to pseudo-solidify liquid electrolytes to boost the mechanical strength without hampering its liquid-like ionic conductivity. Herein, we break this deadlock by proposing a new strategy: arresting the ionic liquids inside the nano-

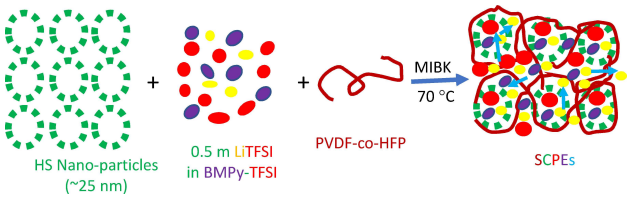

Scheme 1. Fabrication of SCPEs and probable Li-ion transport mechanism is indicated by the arrowhead in which Li-ion and other ions migrate from one localized nanodomains created by HS nanoparticles to another through the free volume created by frustrated packing of the polymer chain in the presence of HS nanoparticles.

spherical prison offered by the nanoarchitecture from HS (Scheme 1). Simultaneously boosting mechanical strength coupled with fast ion conduction is the core concept of this new strategy. Such solid electrolyte is fabricated by confining ionic liquids 1-butyl-1-methylpyrrolidinium bis(trifluoromethanesulfonimide) (BMPy-TFSI) together with lithium bis(trifluoromethanesulfonimide) salt (LiTFSI) in the nanocavity of HS dispersed in the matrix of poly(vinylidene fluoride-co-hexafluoropropylene) (PVDF-co-HFP). Thus fabricated new solid electrolytes were named as solid composite polymer electrolytes (SCPEs). Synthetic methods and the fabrication procedure of SCPEs are explained in the supplementary information. The unique feature of the present work compared with the literature[15] is that, for the first time, we used the uniquely designed HS nanospheres and demonstrated the formation of ionic liquid-rich nanodomain in the membrane, which was not shown in the prior works of literature. Thus, formed ionic liquid-rich nanodomain provides the non-disturbing nanochannel for fast ion conduction and enhances the mechanical strength. Previous work reported the use of silica, titania for the fabrication of composite membrane/polymer gel/ionogel showing the enhancement of ionic conductivity at the expense of mechanical strength, simultaneous boosting of ionic conductivity with robust mechanical strength is the novelty of the present work.

The surface morphology of SCPEs and distribution of HS was investigated by field emission scanning electron microscopy (SEM), transmission electron microscopy (TEM), and energy dispersive spectroscopy (EDS) mapping. Figure 1a shows that the HS nanoparticles have an average diameter of ~25 nm with a ~4 nm wall thickness, consistent with a previous report.[1e] The BET surface area of HS particles is ~616 m^2/g determined by N_2-sorption isotherm. The adsorption-desorption isotherm and corresponding Barret-Joyner-Halenda (BJH) pore-size distribution plot is given in Figures S1a and S1b. Figures 1b and 1c show that HS nanoparticles are uniformly distributed in the matrix of SCPEs-HS4, supported by the uniform distribution of Si, O, N, S of the key components of HS and BMPy-TFSI in Figure S2. The SCPEs-HS4 membrane remains optically transparent, even after loading HS (Figure S3). As demonstrated in the previous work[1e] and Figure S4, the HS nanospheres can confine ionic liquid electrolytes inside their cavities through capillary action. The trapped ionic liquid not only enhances ionic conductivity through the network of porous nanochannel created by interconnected HS but also enhances the mechanical strength by decreasing the plasticization effect of the ILs to the polymer matrix, as shown later. It has also been demonstrated that the specific surface area of the ceramic fillers plays a significant role in the electrochemical performance, that is, smaller particle size offers not only larger surface area but also better battery cycling performance.[11b]

The possible interaction and complexation among the HS, ILs, and polymer matrix were investigated by infrared (IR) spectroscopy. Figure 2 shows the FT-IR spectra of HS, BMPy-TFSI, PVDF-co-HFP, and SCPEs without and with HS. As shown in Figure 2c, pure PVDF-co-HFP contains a crystalline (α) phase appearing at 532, 612, 762, 795 and 974 cm^{-1} while the spectral band around 870 cm^{-1} represents an amorphous (β) phase, indicating PVDF-co-HFP is a semi-crystalline polymer. Although most peaks of PVDF-co-HFP are shielded by those of BMPy-TFSI due to the overlap of their spectra, there is still apparent evidence of their interaction and complexation. For example, the CF_2 symmetric stretching vibration peak shifts from 870 cm^{-1} to 880 cm^{-1}, and the scissoring vibration peak of vinylidene changes from a doublet to a single peak and shifts from a central position of 1390 cm^{-1} to 1410 cm^{-1} (Figure 2 and Figure S5). Similarly, the disappearances of a peak at 974 cm^{-1} for C–F stretching vibration indicates the greater degree of the amorphous state due to complexation with IL, HS, LiTFSI, and polymer backbone. In addition, the interactions introduce a new peak at 1640 cm^{-1} (Figure S5), possibly due to C=C double bond formation by partial dehydro-fluorination of PVDF-co-HFP.[8b,11b]

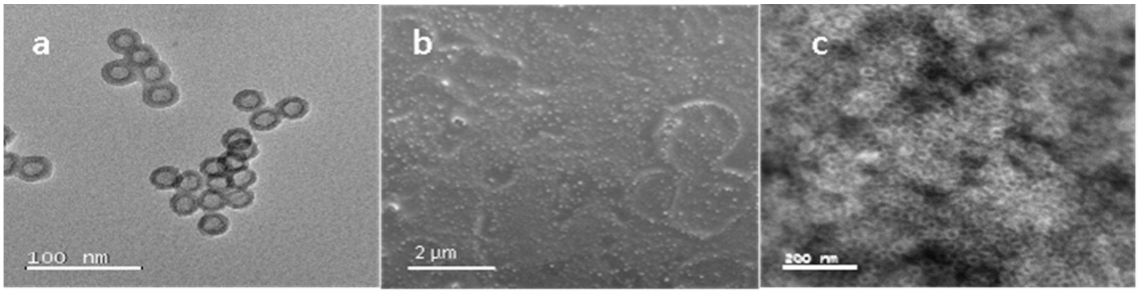

Figure 1. (a) TEM images of hollow silica spheres (HS); (b) SEM and (c) TEM images of SCPEs-HS4 electrolyte membrane showing the uniform distribution of HS in the polymer matrix.

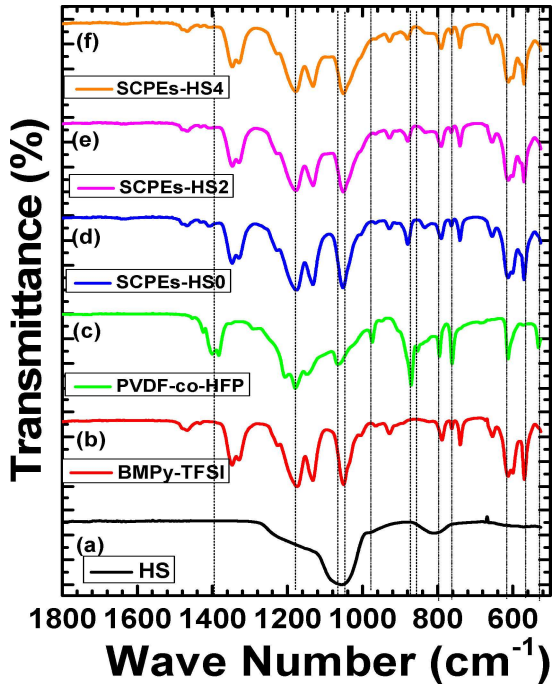

Figure 2. FT-IR spectra of (a) HS; (b) BMPy-TFSI; (c) PVDF-co-HFP; (d) SCPEs-HS0; (e) SCPEs-HS2; and (f) SCPEs-HS4.

The thermogravimetric analysis (TGA) (Figure S6) demonstrates the thermal stability of the SCPEs. The decomposition temperatures of PVDF-co-HFP and BMPy-LiTFSI are 480 and 410 °C, while those of SCPEs-HS0 and SCPEs-HS4 are approximately 400 °C, respectively. The overall high thermal stability of SCPEs demonstrates their suitability for high-temperature operation. Figure 3 shows differential scanning cal orimetry (DSC) heating traces of PVDF-co-HFP, IL, and SCPEs. The DSC trace of BMPy-LiTFSI is similar to that reported in the literature,[16] except that the T_g of −87 °C cannot be shown due to the limitation of the instrument.[17] However, with the addition of 0.5 m LiTFSI, a T_g of −79.35 °C is observed (Figure 3 and Figure S7).

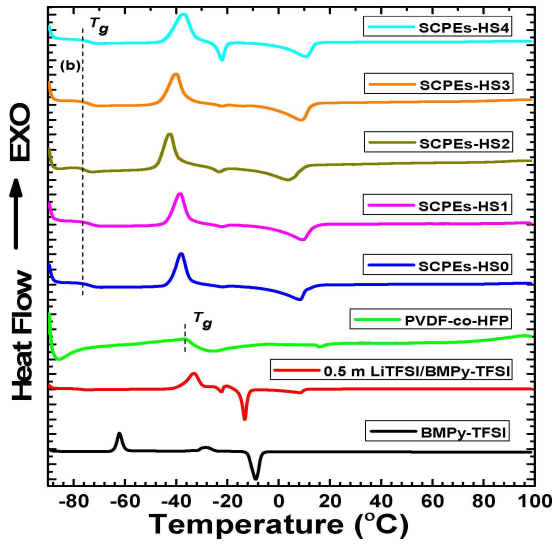

Figure 3. DSC heating traces for PVDF-co-HFP and SCPEs under nitrogen at a heating rate of 5 °C/min.

Generally, the dominant feature of the SCPEs membranes comes from the ionic liquid electrolyte, and the small amount of PVDF-co-HFP (~16–20 wt%) has a negligible effect on the physical properties of the SCPEs.[18] In addition, it seems that the addition of HS to the IL electrolyte and SCPEs has little effect on their T_g (Table S1). The T_g increases slightly with the increasing amount of HS in ionic liquids, which can be attributed to the effect of HS that trapped some ionic liquids. The amount of HS is small (1–4%) comparing to ionic liquids; due to this, it does not have pronounced effects on T_g. However, in the semicrystalline polymer matrix, T_g decreases with the addition of HS due to polymer filler attractive interaction.[19] It may be because of these two counteractive effects; the addition of HS to SCPEs has little effects on the T_g. Therefore, DSC measurements clearly indicate that the segmental motion of the polymer chain is not the major cause of enhanced ionic conductivity.

Figure 4 shows that the tensile strength of the SCPEs were all much higher than that without HS filler. The increase of

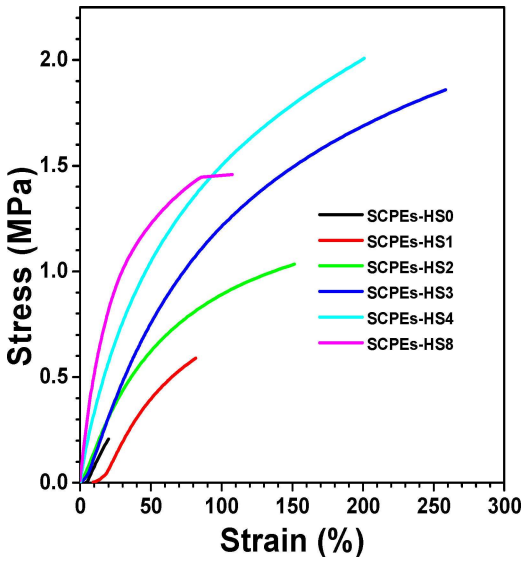

Figure 4. Tensile strength measurement of the SCPEs on a TA Q800 DMA analyzer using controlled force method with 0.1 N/min.

mechanical strengths with the addition of nanoparticles was as expected, which may be attributed to the strong interaction and complexation of HS nanoparticles with the polymer backbone and BMPy-TFSI (supported by IR results), and the decreasing plasticizing effect of the ionic liquid electrolyte as it can be stored in the hollow cavities of HS.[1e,11b, 20] For example, the tensile strength of the SCPEs increased from 0.2 MPa to 2.1 MPa when HS increased from 0 to 4 wt.%, confirming the effect of the HS nanoparticles to improve the tensile properties of the SCPEs. Further increase of HS content to 8 wt.% decreased the tensile strength, which might be due to an

aggregation of HS particles that hinders their homogeneous interaction with the polymer chains.

The temperature-dependent ionic conductivities of the SCPEs were measured and modeled by the Vogel-Fulcher-Tammann (VFT) equation (VFT parameters are tabulated in Table S2).[9c,21] The ionic conductivity increased with increasing HS content, and SCPEs-HS4 exhibited high ionic conductivities of 0.5 and 3.1 mS cm^{-1} at 20 °C and 60 °C, respectively (Figure 5a). The significantly higher ionic conductivities of SCPEs

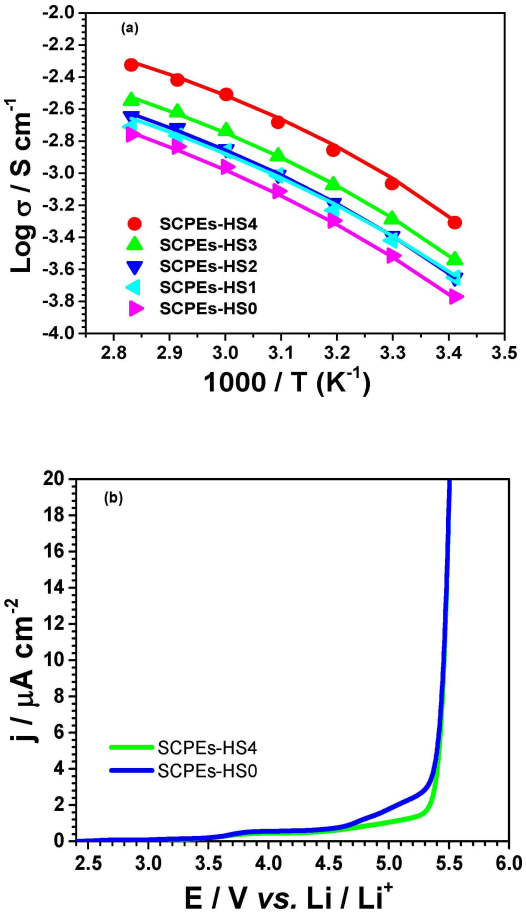

Figure 5. (a) Temperature-dependent ionic conductivity of SCPEs, where solid lines are obtained from VFT fit and marks are experimental data; (b) Linear sweep voltammetry of Li||SCPEs||Pt cell at a scan rate of 10.0 mV/s.

with HS than those without HS could be explained by the following unique nanoarchitecture of the HS incorporated in the SCPEs. First, the presence of polymer matrix in the electrolyte impedes ion conduction of the ionic liquid electrolyte, as is evidenced by the lower ionic conductivity of the gel electrolytes than that of the pure IL electrolyte. Similarly, the ionic conductivity of the polymer gel electrolytes increases with the increasing amount of ILs (Figure S8a).[22] Second, the ionic conductivity of SCPEs with HS is much higher than that with the same amount of solid silica spheres of comparable sizes (SS, ~22 nm), i.e., SCPEs-HS4 vs. SCPEs-SS4 in Figure S8b. Third, as shown in Figure 1, HS is homogeneously distributed in the polymer matrix, creating non-disturbing nanodomains of the ionic liquids strongly confined inside the HS, facilitating the fast ion conduction through nanochannels of interconnected HS particles. This fact is corroborated by the slight decrease in ionic conductivity of IL-HS dispersion because monodisperse HS impede the Li-ion transport through IL (Figure S9). Therefore, the increased ionic conductivities of SCPEs can only be attributed to the hollow architecture of HS, creating nanodomains of IL that provide the nanochannels for fast ion conduction which will be hindered by the polymer chains if no HS is incorporated. This result is a significant achievement that demonstrates that nanoconfinement of ILs does not restrict the liquid dynamics and mobility of the ILs.[12f] The fitting of observed ionic conductivity using the VFT equation shows that the lower activation energy is always correlated with higher ionic conductivity.[21] For example, SCPEs-HS4 had the lowest activation energy (0.95 kJ/mol) and exhibited the highest ionic conductivity.

Figure 5b shows linear sweep voltammograms of SCPEs with and without HS. Both electrolytes showed significant oxidation above 5.3 V vs. Li/Li$^+$. However, the SCPEs with HS had much lower current density than those without HS when the voltage was higher than 4.5 V, suggesting the presence of HS effectively improves the electrochemical stability of the SCPEs *via* effective complexation and interaction between polymer, ILs, and HS, as is evidenced by the FT-IR study (Figure 2) and the mechanical measurement (Figure 4).

Figures 6a and 6b show the performance of the Li|SCPEs-HS4|Li cells at current densities of 0.05 mA cm^{-2} at RT and 0.15 mA cm^{-2} at 60 °C, respectively. The higher voltage under lower current density at RT than that under higher current density at 60 °C was mainly due to its lower ionic conductivity at RT. Nonetheless, both cells maintained a stable voltage profile after 700 hrs, suggesting that SCPEs-HS4 has excellent stability towards lithium to ensure long cell life without short-circuiting. Figures S10a and S10b show the performances of the Li|SCPEs-HS0|Li under the identical condition for Li|SCPEs-

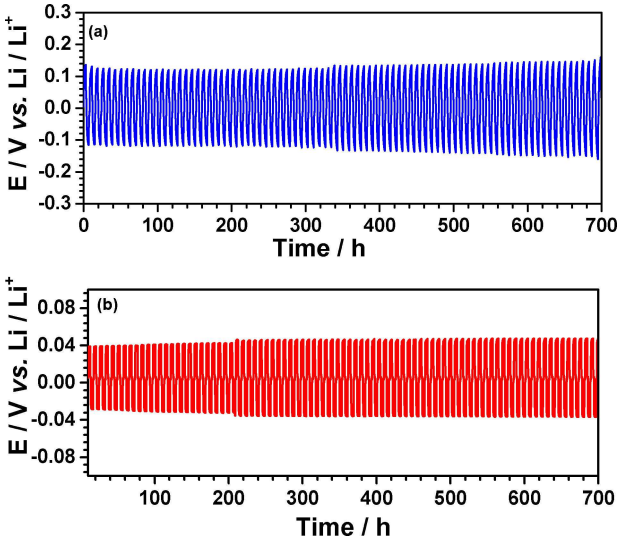

Figure 6. Cyclic performance of Li|SCPEs-HS4|Li cells at a current density of 0.05 mA cm^{-2} at room temperature (a) and 0.15 mA cm^{-2} at 60 °C (b).

HS4 | Li at RT and 60 °C, respectively. At RT, the performance of the Li | SCPEs-HS0 | Li symmetrical cell is similar to that of SCPEs-HS4, whereas at 60 °C, Li | SCPEs-HS0 | Li exhibits the fluctuating voltage profile with spikes after 30 hrs indicating short-circuit because of its weak mechanical strength. This result indicates that incorporation of HS boosts the mechanical strength and electrode compatibility.

Electrochemical impedance spectroscopy (EIS) analysis shows that SCPEs-HS4 exhibited excellent electrode compatibility, as shown in Figure S11. Initially, impedance slightly increased and stabilized after 35 days and remained stable throughout the experiment time. These experiments clearly indicate that SCPEs-HS4 is mechanically robust and electrode-compatible to stabilize the cell, preventing from short-circuiting in long term battery cycling.

In summary, mechanically robust with fast ion-conducting solid electrolytes were successfully fabricated using HS with unique architecture. The hollow spheres with porous silica walls strongly confined the large amounts of ILs electrolytes, maintaining the mechanical robustness through interaction and complexation, whereas the interconnected silica network with the ILs-filled scaffold provided the nanochannels for fast ion conduction. Thus, fabricated SCPEs-HS4 is flexible, optically transparent, and exhibited a superior ionic conductivity of 0.5 and 3.1 mS cm^{-1} at RT and 60 °C, respectively. Symmetric Li | | Li cell experiments exhibited the mechanical strength of the membrane towards lithium dendrite suppression. Excellent compatibility towards lithium was verified by EIS study, indicating that these membranes are stable and suitable for long-term operation of LMBs. Furthermore, superior ionic conductivity coupling with mechanical robustness make SCPEs an ideal candidate for the commercialization of LMBs.

Experimental Section

Materials

PVDF-co-HFP (Aldrich, $M_n \sim 130{,}000$), methyl isobutyl ketone (MIBK, Acros, 99.5% analysis grade), LiTFSI, triblock copolymer Pluronic F-127 ($M_n \sim 12{,}000$), 1,3,5-trimethylbenzene, K_2SO_4, tetramethoxysilane, (3-mercaptopropyl)trimethoxysilane, 1-methylpyrrolidine, and 1-bromobutane were purchased from Sigma-Aldrich and used as received.

Synthesis of Hollow Silica (HS) Spheres

HS spheres were synthesized by following the published procedures.[1e,23] Briefly, triblock copolymer F-127 (1.00 g), 1,3,5-trimethylbenzene (1.00 g), and K_2SO_4 (0.87 g) were dissolved in de-ionized water (60.0 ml) and stirred at 13.5 °C for 4 hours. Then tetramethoxysilane (2.43 g) and (3-mercaptopropyl) trimethoxysilane (0.78 g) were added. After stirring at 13.5 °C for 24 hours, the mixture was transferred into a Teflon-lined autoclave and aged for 24 hours at 100 °C. The formed precipitate was collected by filtration, washed with DI water, and dried at 100 °C. Finally, it was calcinated at 550 °C for 10 hours to obtain HS nanospheres.

Synthesis of 1-Butyl-1-methylpyrrolidinium bis (trifluoromethanesulfonyl)imide (BMPy-TFSI)

Room temperature ionic liquid BMPy-LiTFSI was synthesized following the published procedure.[24] 1-methyl pyrrolidine (32.01 g, 375.89 mmol) was charged in a 250.00 mL round-bottom flask cooled in an ice bath, followed by slow addition of 1-bromobutane 56.67 g (413.57 mmol) under stirring. After addition, the reaction was continued for three days under nitrogen. The obtained solid was washed with diethyl ether (3×50 mL). The solvent was removed on a rotary evaporator and dried under high vacuum for 24 hours to obtain 1-butyl-1-methylpyrrolidinium bromide (BMPy-Br) (75.98 g, 85.7%). Its structure was confirmed by ^{1}H-NMR and ^{13}C-NMR.[25] ^{1}H NMR (400 MHz, DMSO-d_6) δ 3.54–3.35 (m, 4H), 3.34 (t, J = 7.8 Hz, 2H), 3.00 (s, 3H), 2.07 (br s, 4H), 1.67 (quint, J = 7.8 Hz, 2H), 1.33–1.21 (m, 2H), 0.92 (t, J = 7.4 Hz, 3H). ^{13}C NMR (100 MHz, DMSO-d_6) δ 63.3, 62.7, 47.4, 24.9, 21.0, 19.3, 13.5). Before ion exchange, BMPy-Br was decolorized using activated charcoal. Thus, BMPy-Br (75.98 g, 342.02 mmol) was dissolved in deionized (DI) water (160.00 mL) and heated to reflux with activated coconut charcoal (13.0 g) for 12 hrs. The solution was cooled, filtered, and LiTFSI (108.00 g, 376.2 mmol) dissolved in DI water (100 mL) was slowly added under vigorous stirring for 12 hrs to ensure complete anion exchange. The mixture was extracted with dichloromethane, and the combined organic layer was washed with DI water multiple times and dried over magnesium sulfate. The solution was filtered, and the solvent was removed to obtain BMPy-TFSI. Before use, BMPy-TFSI was further dried under high vacuum at 65 °C for 48 hrs. ^{1}H-NMR (400 MHz, DMSO-d_6) δ 3.52–3.35 (m, 4H), 3.32–3.25 (m, 2H), 2.97 (s, 3H), 2.08 (br s, 4H), 1.68 (quint, J = 7.8 Hz, 2H), 1.38–1.25 (m, 2H), 0.93 (t, J = 7.3 Hz, 3H). ^{13}C NMR (100 MHz, DMSO-d_6) δ 119.5 (q, J_{C-F} = 321.9 Hz, TFSI), 63.4, 62.9, 47.5, 24.9, 21.1, 19.3, 13.5).

Fabrication of SCPEs

SCPEs were fabricated by a solution casting method, as illustrated in Scheme 1. Before fabrication of SCPEs, HS and solid silica (SS) nanoparticles were dried at 400 °C and LiTFSI was dried at 150 °C under vacuum to remove moisture. A calculated amount of PVDF-co-HFP and HS were added in a 20.00 mL scintillation vial and mixed with 0.5 m LiTFSI in BMPy-TFSI (80% by weight of PVDF-co-HFP and HS) with methyl isobutyl ketone (MIBK) as the solvent. The mixture was heated at 70 °C for 12 hrs, and the resulting homogeneous solution was cast on a glass Petri dish. The solvent was evaporated slowly under the nitrogen atmosphere at room temperature. The obtained SCPEs were dried at 110 °C under vacuum for a week to ensure complete solvent removal. For comparison, SCPEs with and without HS particles were all prepared and labeled as SCPEs-HSx, where x = 0%, 1%, 2%, 3%, 4%, and 8% representing the weight of HS present in SCPEs. In addition, SCPEs with 80% IL (SCPEs-HS0) and 70% IL without HS (SCPEs-IL70) were also prepared to investigate the IL effect on ionic conductivity. Furthermore, SCPEs with four wt.% SS nanoparticles (av. size ~20 nm) (SCPEs-SS4) was prepared to investigate the effect of silica architecture on ionic conductivity.

Characterization

Infrared (IR) spectroscopy was carried out on a Nicolet IS50 FT-IR (ATR) spectrometer in the range of 4000–500 cm^{-1}. The ^{1}H and ^{13}C NMR spectra were obtained on a JEOL 400 YH spectrometer (400 MHz) with DMSO-d_6 as the solvent, and the chemical shifts were referenced to the residual solvent. The surface morphology of SCPEs was investigated by scanning electron microscopy (SEM), and the distribution of HS was investigated by energy dispersive spectroscopy (EDS) mapping. Differential scanning calorimetry

(DSC) analysis was performed on a TA DSC Q100 under continuous flow of nitrogen. The samples were first cooled to and equilibrated at −90 °C and then heated to 100 °C at a heating rate of 10 °C/min, followed by quenching to and equilibrated at −90 °C again and heated to 100 °C at a heating rate of 10 °C/min. The second scan was used to estimate the glass transition temperature (T_g). Thermogravimetric analysis (TGA) was carried out on a TGA Q50 analyzer under nitrogen flow. All the samples were isothermally held at 20 °C for 30 minutes and heated to 600 °C at a heating rate of 10 °C/min.

Stress–strain properties were measured on a dynamic mechanical analyzer (DMA Q800). The polymer membrane was cut into a rectangular shape (4.0 mm × 3.0 mm) with thickness approximately 0.1 mm for the measurement. Stress–strain analysis was conducted under controlled force mode at 25 °C with a force ramp rate of 0.1 N min^{-1}.

Electrochemical Measurements

Ionic conductivity (σ) was measured using alternating current (AC) electrochemical impedance spectroscopy (EIS) on Biologic VSP over frequency ranging from 200 KHz to 100 mHz with a 10 mV perturbation potential. The measurement was carried out using Swagelok cells, which were assembled inside an argon-filled glove box by sandwiching the SCPEs between two stainless steel electrodes. The cells were equilibrated at each temperature for 45 minutes before measurement. The ionic conductivity (σ) of the SCPEs was calculated by using the following equation [Eq. (1)]:

$$\sigma = \frac{l}{A\,R} \tag{1}$$

Where R is the SCPEs resistance, A is the surface area, and l is the thickness of the membranes.

The temperature dependence of ionic conductivities of SCPEs can be well described by the Vogel-Fulcher-Tammann (VFT) equation:[9c,21]

$$\sigma = \sigma_o \exp\left(\frac{-E_a}{R(T - T_o)}\right) \tag{2}$$

Where σ_o, E_a, and R are the frequency pre-factor, activation energy, and universal gas constant, respectively. T_o is an empirical constant, usually 10–50 °C below the glass transition temperature.

Linear sweep voltammetry (LSV) was carried out using platinum as working electrode and Li as counter electrode from 2.0 V to 6.0 V vs. Li/Li$^+$ with a scan rate of 10 mV/s. Symmetric Li||SCPEs||Li cells, which were assembled by sandwiching SCPEs between two lithium disks as a non-blocking electrode in an argon-filled glove box, were used to study interfacial stability. Interfacial stability was measured by cycling the symmetric Li cells with a sequence of 3 hours charge, 1 hr rest, and 3 hrs discharge, and 1 hr rest.[26]

Acknowledgements

This work was supported by the U.S. Department of Energy, Office of Science, Office of Basic Energy Sciences, Materials Sciences and Engineering Division under contract number DE-AC05-00OR22725. TEM analysis of this work used the resources of the Center for Functional Nanomaterials, which is a U.S. Department of Energy, Office of Science facility, Brookhaven National Laboratory under contract number DE-SC0012704.

Conflict of Interest

The authors declare no conflict of interest.

Keywords: lithium metal batteries · solid composite electrolytes · poly(vinylidene fluoride-co-hexafluoropropylene) · ionic liquids · hollow silica spheres

[1] a) M. Armand, J. M. Tarascon, *Nature* **2008**, *451*, 652; b) D. Lin, Y. Liu, Y. Cui, *Nat. Nanotechnol.* **2017**, *12*, 194; c) J. M. Tarascon, M. Armand, *Nature* **2001**, *414*, 359; d) M. S. Whittingham, *Chem. Rev.* **2004**, *104*, 4271; e) J. Zhang, Y. Bai, X.-G. Sun, Y. Li, B. Guo, J. Chen, G. M. Veith, D. K. Hensley, M. P. Paranthaman, J. B. Goodenough, S. Dai, *Nano Lett.* **2015**, *15*, 3398; f) Q. Zhang, K. Liu, F. Ding, X. Liu, *Nano Res.* **2017**, *10*, 4139.

[2] a) Y. C. Li, G. M. Veith, K. L. Browning, J. H. Chen, D. K. Hensley, M. P. Paranthaman, S. Dai, X. G. Sun, *Nano Energy* **2017**, *40*, 9; b) B. Liu, Q. Li, M. H. Engelhard, Y. He, X. Zhang, D. Mei, C. Wang, J.-G. Zhang, W. Xu, *ACS Appl. Mater. Interfaces* **2019**, *11*, 21496; c) I. A. Shkrob, B. Han, R. Sahore, A. P. Tornheim, L. Zhang, D. P. Abraham, F. Dogan, Z. Zhang, C. Liao, *Chem. Mater.* **2019**, *31*, 2459; d) W. Xu, K. Zhao, W. Huo, Y. Wang, G. Yao, X. Gu, H. Cheng, L. Mai, C. Hu, X. Wang, *Nano Energy* **2019**, *62*, 275.

[3] a) K. Zhang, G.-H. Lee, M. Park, W. Li, Y.-M. Kang, *Adv. Energy Mater.* **2016**, *6*, 1600811; b) C. Niu, H. Pan, W. Xu, J. Xiao, J.-G. Zhang, L. Luo, C. Wang, D. Mei, J. Meng, X. Wang, Z. Liu, L. Mai, J. Liu, *Nat. Nanotechnol.* **2019**, *14*, 594; c) W. Alkarmo, F. Ouhib, A. Aqil, J.-M. Thomassin, J. Yuan, J. Gong, B. Vertruyen, C. Detrembleur, C. Jérôme, *Macromol. Rapid Commun.* **2019**, *40*, 1800545; d) B. P. Thapaliya, C. J. Jafta, H. Lyu, J. Xia, H. M. Meyer Iii, M. P. Paranthaman, X.-G. Sun, C. A. Bridges, S. Dai, *ChemSusChem* **2019**, *12*, 1316.

[4] W. Xu, J. Wang, F. Ding, X. Chen, E. Nasybulin, Y. Zhang, J.-G. Zhang, *Energy Environ. Sci.* **2014**, *7*, 513.

[5] a) S. Liang, U. H. Choi, W. Liu, J. Runt, R. H. Colby, *Chem. Mater.* **2012**, *24*, 2316; b) Q. Pan, D. Barbash, D. M. Smith, H. Qi, S. E. Gleeson, C. Y. Li, *Adv. Energy Mater.* **2017**, *7*, 1701231; c) S. Zekoll, C. Marriner-Edwards, A. K. O. Hekselman, J. Kasemchainan, C. Kuss, D. E. J. Armstrong, D. Y. Cai, R. J. Wallace, F. H. Richter, J. H. J. Thijssen, P. G. Bruce, *Energy Environ. Sci.* **2018**, *11*, 185; d) Y. T. Li, B. Y. Xu, H. H. Xu, H. N. Duan, X. J. Lu, S. Xin, W. D. Zhou, L. G. Xue, G. T. Fu, A. Manthiram, J. B. Goodenough, *Angew. Chem. Int. Ed.* **2017**, *56*, 753; e) X. Y. Yao, D. Liu, C. S. Wang, P. Long, G. Peng, Y. S. Hu, H. Li, L. Q. Chen, X. X. Xu, *Nano Lett.* **2016**, *16*, 7148; f) F. Han, J. Yue, C. Chen, N. Zhao, X. Fan, Z. Ma, T. Gao, F. Wang, X. Guo, C. Wang, *Joule* **2018**, *2*, 497; g) D. T. Hallinan, I. Villalaunega, N. P. Balsara, *MRS Bull.* **2018**, *43*, 759; h) K. Fu, Y. Gong, J. Dai, A. Gong, X. Han, Y. Yao, C. Wang, Y. Wang, Y. Chen, C. Yan, Y. Li, E. D. Wachsman, L. Hu, *Proc. Mont. Acad. Sci.* **2016**, *113*, 7094; i) J. Li, C. Ma, M. Chi, C. Liang, N. J. Dudney, *Adv. Energy Mater.* **2015**, *5*, 1401408.

[6] J. C. Li, C. Ma, M. F. Chi, C. D. Liang, N. J. Dudney, *Adv. Energy Mater.* **2015**, *5*.

[7] D. T. Hallinan, I. Villalaunega, N. P. Balsara, *MRS Bull.* **2018**, *43*, 759.

[8] a) W. Liu, N. Liu, J. Sun, P.-C. Hsu, Y. Li, H.-W. Lee, Y. Cui, *Nano Lett.* **2015**, *15*, 2740; b) X. Zhang, T. Liu, S. Zhang, X. Huang, B. Xu, Y. Lin, B. Xu, L. Li, C.-W. Nan, Y. Shen, *J. Am. Chem. Soc.* **2017**, *139*, 13779.

[9] a) R. C. Agrawal, G. P. Pandey, *J. Phys. D* **2008**, *41*, 223001; b) Y. Tong, H. Lyu, Y. Xu, B. P. Thapaliya, P. Li, X.-G. Sun, S. Dai, *J. Mater. Chem. A* **2018**, *6*, 14847; c) E. Quartarone, P. Mustarelli, *Chem. Soc. Rev.* **2011**, *40*, 2525; d) H. Zhang, C. Li, M. Piszcz, E. Coya, T. Rojo, L. M. Rodriguez-Martinez, M. Armand, Z. Zhou, *Chem. Soc. Rev.* **2017**, *46*, 797; e) M. Watanabe, M. Kanba, K. Nagaoka, I. Shinohara, *J. Appl. Polym. Sci.* **1982**, *27*, 4191; f) J. Vondrák, X. Sedlařı, X. M. Ková, J. Velická, B. Klápště, V. Novák, X. Tězslav, J. Reiter, *Electrochim. Acta* **2001**, *46*, 2047; g) S. Feng, D. Shi, F. Liu, L. Zheng, J. Nie, W. Feng, X. Huang, M. Armand, Z. Zhou, *Electrochim. Acta* **2013**, *93*, 254; h) L. Porcarelli, A. S. Shaplov, F. Bella, J. R. Nair, D. Mecerreyes, C. Gerbaldi, *ACS Energy Lett.* **2016**, *1*, 678.

[10] F. Croce, G. B. Appetecchi, L. Persi, B. Scrosati, *Nature* **1998**, *394*, 456.

[11] a) A. M. Stephan, K. S. Nahm, *Polymer* **2006**, *47*, 5952; b) P. M. Shanthi, P. J. Hanumantha, T. Albuquerque, B. Gattu, P. N. Kumta, *ACS Appl. Energy Mater.* **2018**, *1*, 483; c) D. Zhang, R. Li, T. Huang, A. Yu, *J. Power Sources* **2010**, *195*, 1202.
[12] a) M. Armand, F. Endres, D. R. MacFarlane, H. Ohno, B. Scrosati, *Nat. Mater.* **2009**, *8*, 621; b) Q. Yang, Z. Zhang, X.-G. Sun, Y.-S. Hu, H. Xing, S. Dai, *Chem. Soc. Rev.* **2018**, *47*, 2020; c) M. Watanabe, M. L. Thomas, S. Zhang, K. Ueno, T. Yasuda, K. Dokko, *Chem. Rev.* **2017**, *117*, 7190; d) C. J. Jafta, C. Bridges, L. Haupt, C. Do, P. Sippel, M. J. Cochran, S. Krohns, M. Ohl, A. Loidl, E. Mamontov, P. Lunkenheimer, S. Dai, X.-G. Sun, *ChemSusChem* **2018**, *11*, 3512; e) X.-G. Sun, S. Dai, *Electrochim. Acta* **2010**, *55*, 4618; f) J. Le Bideau, L. Viau, A. Vioux, *Chem. Soc. Rev.* **2011**, *40*, 907.
[13] N. Chen, Y. Dai, Y. Xing, L. Wang, C. Guo, R. Chen, S. Guo, F. Wu, *Energy Environ. Sci.* **2017**, *10*, 1660.
[14] a) S. Chen, K. Wen, J. Fan, Y. Bando, D. Golberg, *J. Mater. Chem. A* **2018**, *6*, 11631; b) J.-F. Wu, X. Guo, *J. Mater. Chem. A* **2019**, *7*, 2653; c) J.-F. Wu, X. Guo, *Small* **2019**, *15*, 1804413; d) J. Zhang, J. Yang, T. Dong, M. Zhang, J. Chai, S. Dong, T. Wu, X. Zhou, G. Cui, *Small* **2018**, *14*, 1800821.
[15] a) S. Khurana, A. Chandra, *Solid State Ionics* **2019**, *340*, 115027; b) Y. Cheng, S. Lu, R. Zheng, D. Zhang, H. Zhang, *Appl. Surf. Sci.* **2019**, *485*, 119; c) P. M. Shanthi, P. J. Hanumantha, T. Albuquerque, B. Gattu, P. N. Kumta, *ACS Appl. Energy Mater.* **2018**, *1*, 483; d) S. Choudhury, R. Mangal, A. Agrawal, L. A. Archer, *Nat. Commun.* **2015**, *6*, 10101; e) F. Wu, N. Chen, R. Chen, L. Wang, L. Li, *Nano Energy* **2017**, *31*, 9.
[16] a) D. R. MacFarlane, P. Meakin, J. Sun, N. Amini, M. Forsyth, *J. Phys. Chem. B* **1999**, *103*, 4164; b) W. A. Henderson, S. Passerini, *Chem. Mater.* **2004**, *16*, 2881.
[17] X. G. Sun, S. Dai, *Electrochim. Acta* **2010**, *55*, 4618.
[18] A. Martinelli, A. Matic, P. Jacobsson, L. Borjesson, M. A. Navarra, S. Panero, B. Scrosati, *J. Electrochem. Soc.* **2007**, *154*, G183.
[19] a) J. Jordan, K. I. Jacob, R. Tannenbaum, M. A. Sharaf, I. Jasiuk, *Mater. Sci. Eng. A* **2005**, *393*, 1; b) T. Hanemann, D. V. Szabó, *Materials* **2010**, *3*.
[20] Z. Tu, Y. Kambe, Y. Lu, L. A. Archer, *Adv. Energy Mater.* **2013**, *4*, 1300654.
[21] K. M. Diederichsen, H. G. Buss, B. D. McCloskey, *Macromolecules* **2017**, *50*, 3831.
[22] a) C. Liao, X. G. Sun, S. Dai, *Electrochim. Acta* **2013**, *87*, 889; b) Shalu, V. K. Singh, R. K. Singh, *J. Mater. Chem. C* **2015**, *3*, 7305; c) X. W. Li, S. J. Li, Z. X. Zhang, J. Huang, L. Yang, S. Hirano, *J. Mater. Chem. A* **2016**, *4*, 13822.
[23] J. Zhang, S.-H. Chai, Z.-A. Qiao, S. M. Mahurin, J. Chen, Y. Fang, S. Wan, K. Nelson, P. Zhang, S. Dai, *Angew. Chem. Int. Ed.* **2014**, *54*, 932.
[24] A. K. Burrell, R. E. D. Sesto, S. N. Baker, T. M. McCleskey, G. A. Baker, *Green Chem.* **2007**, *9*, 449.
[25] N. L. Lancaster, P. A. Salter, T. Welton, G. B. Young, *J. Org. Chem.* **2002**, *67*, 8855.
[26] Y. Tong, H. Lyu, Y. Xu, B. P. Thapaliya, P. Li, X.-G. Sun, S. Dai, *J. Mater. Chem. A* **2018**, *6*, 14847.

Manuscript received: July 14, 2019
Revised manuscript received: August 23, 2019
Accepted manuscript online: September 3, 2019
Version of record online: September 19, 2019